Electric Power Systems Research 152 (2017) 18–26

Contents lists available at ScienceDirect

Electric Power Systems Research

journal homepage: www.elsevier.com/locate/epsr

Analysis of various inverters feeding induction motors with incipient rotor fault using high-resolution spectral analysis

I. Martin-Diaz[a,b], D. Morinigo-Sotelo[b], O. Duque-Perez[b], P.A. Arredondo-Delgado[a,b], D. Camarena-Martinez[a], R.J. Romero-Troncoso[a,*]

[a] HSPdigital-CATelematica, DICIS, Universidad de Guanajuato, Carr., Salamanca-Valle km 3.5 + 1.8, Palo Blanco, 36885 Salamanca, Guanajuato, Mexico
[b] Elect. Eng. Dept. Escuela de Ingenierias Industriales, Sede Paseo del Cauce, University of Valladolid, Paseo del Cauce, 59, 47011 Valladolid, Spain

ARTICLE INFO

Article history:
Received 5 December 2016
Received in revised form 21 June 2017
Accepted 22 June 2017
Available online 3 July 2017

Keywords:
Condition monitoring
Fault detection
Induction motor
Inverter
Multiple signal classification
Spectral analysis

ABSTRACT

Recently, there has been an increased interest in fault detection on electrical machines in steady-state regimes. Several frequency estimation techniques have been developed to assist the early detection of faults in induction motors, especially in line-fed motors. However, in modern industry, the use of inverters is increasingly present. This paper presents an analysis for comprehending the challenge in detecting incipient rotor faults using the stator current signal under different inverter supplies. The approach is based on the high-resolution technique known as multiple signal classification (MUSIC). In this study, incipient rotor faults in a squirrel-cage rotor, prior to the complete breaking of a rotor bar, are better identified in some inverters than others. The proposed approach finds the adequate MUSIC order that facilitates identification of bar breakage frequencies for early fault detection in each case studied from a wide set of trials. The study has been developed to detect incipient rotor bar breakages in an inverter-fed three-phase induction motor under varying load situations.

1. Introduction

Induction motors (IM) are considered the workhorse of industry, mainly because of their robustness, reliability, and low price. Despite these advantages, they are susceptible to failures and require condition monitoring to carry out effective predictive maintenance practices [1]. Researchers have devoted considerable efforts in the area of Motor Current Signature Analysis (MCSA) [2–5] for IM fault detection (FD) under different conditions that are commonly present in industrial environments. MCSA has many advantages such as being non-invasive, it does not interfere with motor operation, and it is less affected by environmental noise compared to vibration signals. Therefore, MCSA-based approaches provide a reliable monitoring of rotor health. Since spectral analysis techniques are useful to identify faulty patterns in frequency domain, Fast Fourier Transform (FFT) has been widely used [6]. FFT makes use of Discrete Fourier Transform (DFT) using a computationally efficient algorithm [7]. However, it has some drawbacks: it suffers from spectral leakage, lacks a good frequency resolution, and it also produces a noisy spectrum, especially in inverter-fed IM [8], which limits its reliability [9]. Certainly, FFT can be a useful tool when the normal situation of the IM is in steady state. Yet, the current signal is in fact time varying, which makes it more difficult to achieve the steady-state condition for FFT computation, also demanding a long acquisition period and is impractical for low slip applications [10]. Nevertheless, MUSIC and ESPRIT are suited methods for analyzing signals with low SNR [11]. In [10], the Hilbert transform is combined with ESPRIT to perform fault detection on IM operating at low slip to improve BRB fault detection and to overcome the limitations of the FFT. Authors in Ref. [10] stated that ESPRIT has the capacity to avoid spectral leakage and its combined application with the Hilbert transform has given good results to detect a broken rotor bar (BRB) when the fault components are close to the fundamental component [10]. Unlike FFT, MUSIC algorithm can be computed from a much shorter acquisition period and with lower memory requirements to locate BRB frequencies, producing comparable results to those FFT-based methods [12], and this is because the technique can be applied to a narrow frequency band where the BRB components are present. Through decimation on that frequency band, the required sampling rate is reduced and thus, computation time is decreased.

Some key papers in the field [10,13–21] deal with the fault of a BRB. For instance, Kim et al. [18] introduced an axis transformation and average method for detecting a BRB using the current spectrum in an inverter driven induction machine. The results proved to be more effective compared to FFT regarding fault diagnosis sys-

* Corresponding author.
E-mail address: troncoso@hspdigital.org (R.J. Romero-Troncoso).

http://dx.doi.org/10.1016/j.epsr.2017.06.021
0378-7796/

tem costs. Other researchers [16] investigated the generation of specific frequency components related to induction motor faults in inverter-supplied electric drive systems. Also, the authors in Ref. [19] dealt with the diagnosis of rotor faults in closed-loop IM drives. Their main contribution was the use of the inverter to perform an offline test, equivalent to a single-phase rotation test. Ghorbanian et al. [20] reviewed suitable techniques for FD, addressing fault diagnosing procedures with different kinds of supply. This study was focused partly on BRB considering motor supply and condition changes. However, although the detection of a BRB is a milestone in the detection of IM rotor faults, the determination of an incipient BRB still remains a challenging situation in the literature. Early FD is even more difficult in inverter-fed IM [20–22]. Since there are no studies that consider the influence of various types of inverters for dealing with early FD, a wrong conclusion may be drawn by generalizing from the behavior of the hitherto proposed techniques by limiting themselves to only one power supply. Thus, the diagnosis technique utilized must be applied under different supply conditions to show its potential to deal with incipient faults. FD complications in inverter-fed IM may be explained by noise level introduced by the inverter [16–18], which is originated by pulse width modulation (PWM) technique, the control mode [21], and the inverter model or brand. Each inverter model introduces different power conversion harmonics into the stator current spectrum [22]. They contribute to the generation of inter- and sub-harmonics in the stator current, negatively affecting the diagnosis. Consequently, in the case of a partial BRB, differences among inverters may be observed, and it is worth reporting some conclusions about the detectability of this fault in these situations.

The main objective of this paper is to prove the potentiality of high-resolution spectral analysis to detect a BRB at an early stage for different inverter feedings. The analysis is performed by using a considerable number of trials of various inverters to supply an IM, considering several load conditions, ranging from medium to high. Given these load levels, MUSIC has been selected as the analysis method to locate the characteristic spectral components, present at the incipient rotor fault in an inverter-fed IM. The analytical methodology consists of basically three stages: a preprocessing stage that selects the most relevant samples; a high-resolution spectral estimation of the BRB frequencies based on MUSIC; and a third stage for quantifying the fault severity. Experimentation is performed to test the feasibility of this method using an IM and three different inverters.

2. Application of MUSIC to the detection of incipient broken bar fault

As is well known, the BRB-related components are given by Eq. (1), resulting in sidebands around integer harmonics [22]:

$$f_{BRB} = (k \pm 2ns)f_s,\ n = 1, 2, 3, \ldots \tag{1}$$

where s is the per-unit motor slip, and k is the harmonic order.

The MUSIC algorithm estimates the frequency content of a signal using eigenvector decomposition of the autocorrelation matrix. In this method, it is assumed that $x[n]$, the discrete time stator current signal, is a sum of M complex sinusoids with white noise and it can be expressed as follows:

$$x[n] = \sum_{i=1}^{M} \bar{A}_i e^{j2\pi f_i n} + e[n] \tag{2}$$

with

$$\bar{A}_i = |A_i| e^{j\phi_i} \tag{3}$$

and $n = 0,1,2,\ldots, N-1$ where N is the number of sampled data, $|A_i|$ is the magnitude, f_i is the frequency, ϕ_i is the random phase of i-th complex sinusoid, and $e[n]$ is white noise with zero mean and variance σ^2. $\boldsymbol{R_x}$ is the MxM autocorrelation matrix of $x[n]$ and can be expressed as the sum of signal and noise autocorrelation matrices $\boldsymbol{R_s}$ and $\boldsymbol{R_n}$ respectively, as follows:

$$\mathbf{R_x} = \mathbf{R_s} + \mathbf{R_n} = \sum_{i=1}^{m} |A_i|^2 \boldsymbol{e}(f_i)\boldsymbol{e}^H(f_i) + \sigma^2\mathbf{I} \tag{4}$$

where m is the number of frequency components, the exponent H denotes the Hermitian transpose, $\mathbf{I}$ is the identity matrix, and $\boldsymbol{e}^H(f_i)$ is the signal vector given by:

$$\boldsymbol{e}(f_i) = [1 e^{j2\pi f_i} e^{j4\pi f_i} \ldots e^{j2\pi(N-1)f_i}]^T \tag{5}$$

From the orthogonality condition of both subspaces, the MUSIC pseudo-spectrum Q is given by:

$$Q^{MUSIC}(f) = \frac{1}{|\boldsymbol{e}^H(f_i)\boldsymbol{v}_{m+1}|^2} \tag{6}$$

$$\boldsymbol{v}_{m+1} = \sum_{k=m+1}^{M} \boldsymbol{v}_m \boldsymbol{v}_m^H \tag{7}$$

where $\boldsymbol{v}_{m+1}$ is the noise eigenvector and is expressed as in Eq. (7). This expression exhibits the peaks that are at exact frequencies of the principal sinusoidal components, where $\boldsymbol{e}(f)^H \boldsymbol{v}_{m+1} = 0$.

The scalar integer and tuning parameter m, also known as the MUSIC order, is the signal subspace dimension. The performance of the MUSIC algorithm depends on this value, and it determines the dimension of the autocorrelation matrix, which is unknown *a priori*. Indeed, there is no theoretical basis for computing the exact value of m, but a multi-objective optimization method, to address this question, has been proposed in Ref. [15]. Mainly, in the analysis of different inverter feedings, the corresponding autocorrelation matrices should contain high enough eigenvalues for the noise space and should be low enough not to highlight spurious frequencies, all of which performed with a reduced computational time.

3. Methodology and signal processing

A block diagram of the proposed methodology is shown in Fig. 1. First, a one-phase stator current signal is acquired for each power supply and rotor state. Then, band-pass filtering, for limiting those frequencies outside a specific bandwidth, is applied before using the FFT and MUSIC algorithms. Once a sizeable dataset of signals is built from the laboratory experiments, the MUSIC algorithm is tuned, applying it to those signals obtained under different motor loads and rotor conditions.

The band-pass FIR filter designed is based on the Parks–McClellan optimal filter order estimation, which is implemented in the signal processing toolbox of MATLAB©. The band-pass filter parameters are defined as follows: (1) The band-pass frequencies are set at 42 Hz and 58 Hz, respectively, considering that at higher loads, the BRB faulty components are further separated from the fundamental frequency [23], and the maximum slip of the trials at high loads has a per-unit value of 0.065, which corresponds to values of LSH = 43.5 Hz and RSH = 56.5 Hz. The frequencies are chosen based on the highest load level since it is the limiting factor of the frequency band of interest for locating the BRB components within that range; (2) the first and second stop-band frequencies are assigned to be 30 Hz and 70 Hz, respectively. This step rejects those frequencies related to lower and higher harmonics than the fundamental, and (3) the attenuation at the stop-band is set at 40 dB, which requires an order of 32 for the FIR filter. This FIR filter has been designed to allow the observation of the frequencies of interest and to eliminate the switching frequencies of the inverters located in the kHz region.

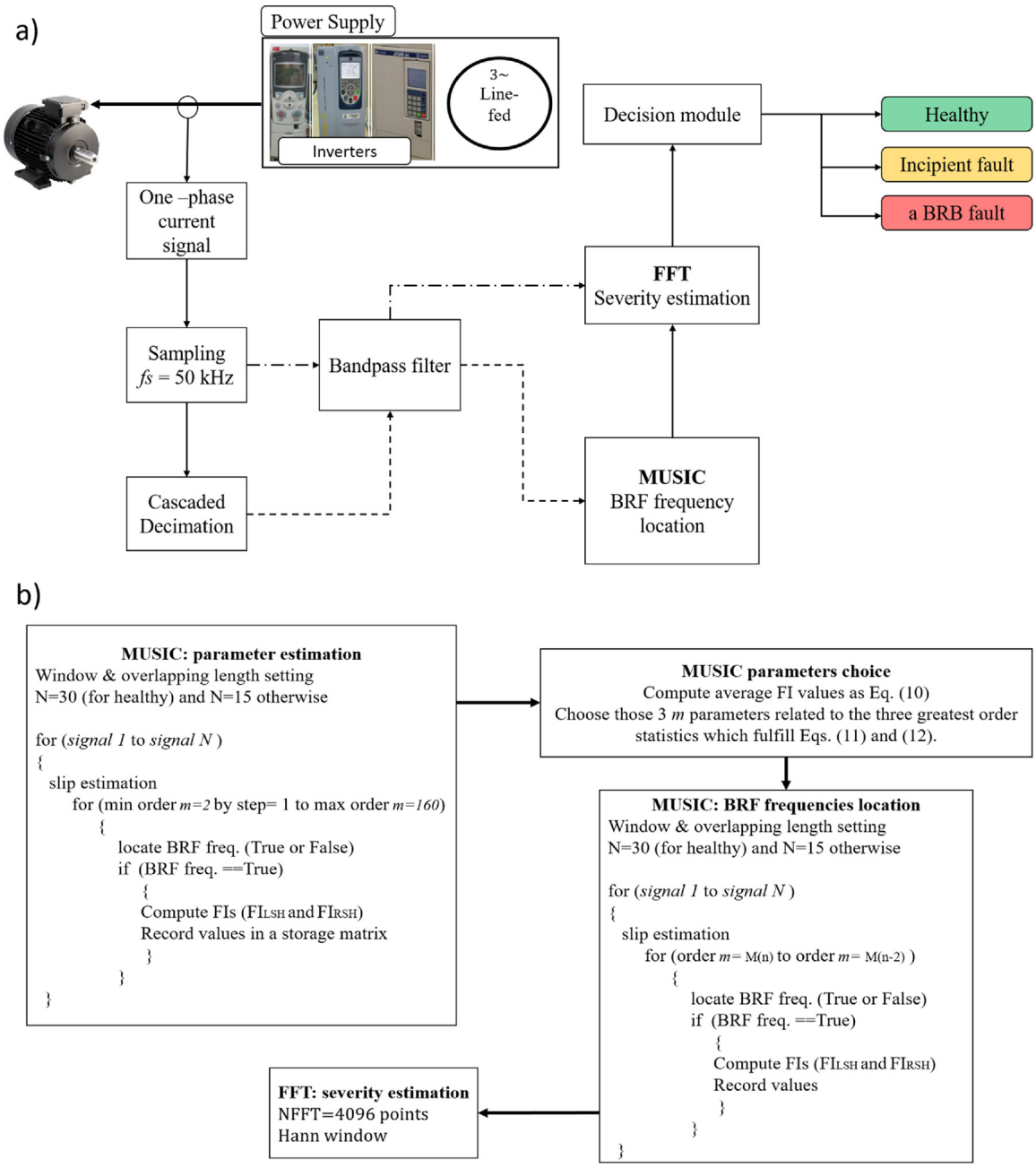

Fig. 1. (a) Block diagram of the proposed method, (b) flowchart with the procedure steps for the rotor severity analysis.

First, the methodology includes the accurate location of BRB frequencies, which is done with MUSIC in a time segment of one second. This is estimated by increasing the time interval from 0.1 s and abovein increments of 0.1 s. When the time interval is 0.5 s or lower, the obtained spectra is as depicted in Fig. 2a for the case of an ABB inverter-fed induction motor at high load, being unable to locate the frequency components clearly. When the time interval is increased to 0.6 s, the results show that the frequency components can be rightly located as shown in Fig. 2b, which establishes the lower detectability limit for the time interval in MUSIC. Nevertheless, to have a safety margin in the location of the fault, a time interval of 1 s is chosen.

Second, the methodology requires the quantification of the BRB frequencies, indicated by the component magnitude, which is done with FFT in a time segment of ten seconds. This is estimated by increasing the time interval from 1 s and above in increments of 1 s. When the time interval is increased to 10 s, the results show that the frequency quantification can be accurately estimated as shown in Fig. 3a. Therefore, with this interval of 10 s and a sampling frequency of 50 kHz, a frequency resolution of 0.1 Hzis achieved. For shorter time segments, the resolution method is poor for the quantification phase, as can be seen in Figs. 3b–c. When the time interval is 5 s or lower, the spectrum obtained shows a lower resolution, being unable to quantify the BRB frequency components clearly. Figs. 3a–c, show the case of an ABB inverter-fed induction motor at high load.

As a result, the signal length is reduced to 5000 samples with a bandwidth of 250 Hz, which includes the frequencies of interest. After the data acquisition stage, the Power Spectral Density (PSD) of the signal is computed by using the FFT algorithm with a Hann window to reduce the spectral leakage effect. These spectra will be shown next for comparison purposes only. The signal process-

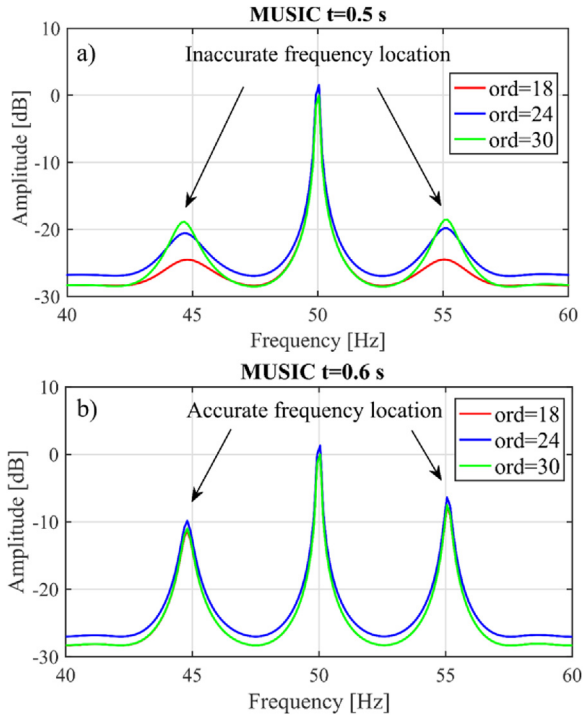

Fig. 2. Influence of the acquisition time interval for frequency location with time segments of (a) 0.5 s, and (b) 0.6 s.

Table 1
Number of data samples for the proposed application.

IM Supply	Load level	Healthy	Partially BRB	Fully BRB
ABB	Medium load	30	15	15
	High load	30	15	15
WEG	Medium load	30	15	15
	High load	30	15	15
TM	Medium load	30	15	15
	High load	30	15	15
Line-fed	Medium load	30	15	15
	High load	30	15	15

ing software has been implemented by using the MATLAB© Signal Processing toolbox. For FFT estimation, the data window length is set to 4096 points. In both cases, the FFT spectrum and the MUSIC pseudo-spectrum are normalized and expressed in dB with respect to the fundamental component. A flowchart of the steps made during the analysis stage is detailed in Fig. 1b. In this study, a sizeable test dataset has been analysed with 30 and 15 stator current signals found to be statistically significant [24]. The signals correspond to a motor in healthy and faulty states, two load levels, and various power supplies, as summarized in Table 1. The detection of the BRB fault using spectral analysis techniques is easier when the load level is high because the distance between the fundamental component and the BRB component is directly proportional to the load. Then, at higher load levels, the separation of the BRB component and the fundamental frequency is greater. For this reason, two load levels were chosen: high and medium, the medium load case offering more challenging conditions for detecting a fault. The BRB is verified by the presence of the left sideband harmonic (LSH) and the right sideband harmonic (RSH), which are frequency components around the fundamental frequency in the current spectrum, as described in Eq. (1).

The tuning parameters of MUSIC are chosen accordingly by means of an iteration loop, which computes a fault index in the

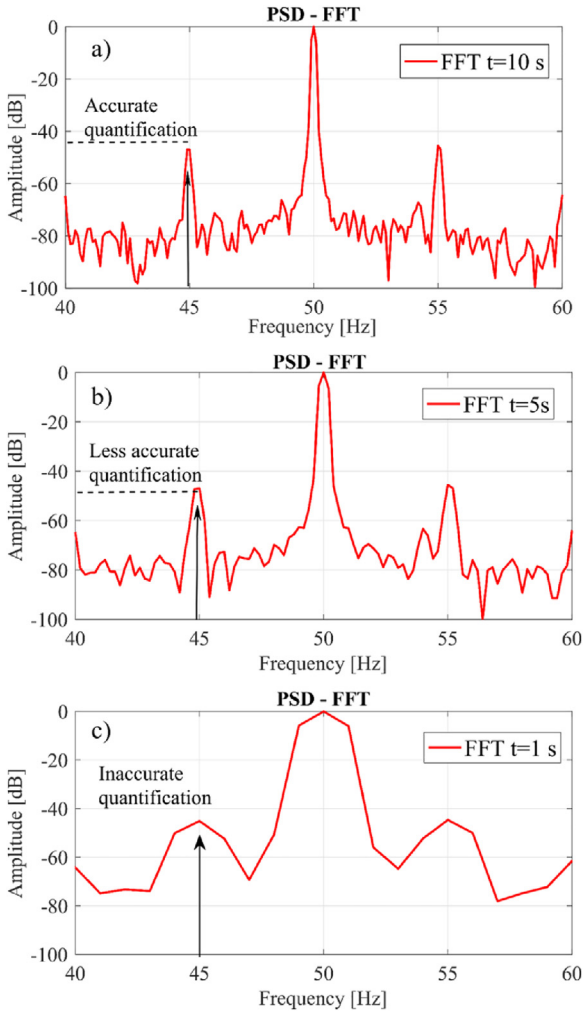

Fig. 3. Influence of the acquisition time for severity quantification with time segments of: (a) 10 s; (b) 5 s, and (c) 1 s.

range of BRB frequencies of interest (see Fig. 1b). The fault index (FI) is defined for the LSH and RSH harmonics as follows:

$$FI_{LSH} = A^M_{f_{LSH}} - \min\left\{A^M_{f_{LSH}}, A^M_{f_1}\right\} \quad (8)$$

$$FI_{RSH} = A^M_{f_{RSH}} - \min\left\{A^M_{f_1}, A^M_{f_{RSH}}\right\} \quad (9)$$

Both *FI* are computed from the MUSIC spectrum as the difference between the peak amplitude values at each characteristic frequency, $A^M_{f_{LSH}}$ and $A^M_{f_{RSH}}$, and the minimum value found between that peak and the fundamental component $A^M_{f_1}$.

As the slips are known, the BRB frequencies can be located by performing a peak search through the stator current PSD around the fundamental component (frequency band of interest). The computational effort is mostly spent on the analysis for every *m* value within the loop, which considers the complete set of experimental signals.

This iterative analysis allows the most appropriate MUSIC orders for the detection of different rotor conditions to be chosen. Within the iterative loop, the fault information is accomplished first by searching for the peaks of interest (f_{BRB} frequencies) in the MUSIC pseudo-spectrum and then, computing the prior fault indexes if the above-mentioned peaks appear in the spectra. The signal faulty information calculated during this processing is stored in a data matrix accordingly. Due to the stochastic nature of the signal, there is no single order for obtaining information related to the early fault

for every signal from the dataset obtained in the laboratory trials. For this reason, three MUSIC orders have been chosen that present better discriminative behavior [15] among rotor states. They are chosen as follows:

1) First, the average of the *FI* (10), computed in Eqs. (8) and (9) for the LSH and RSH respectively, for each rotor state *R*, *i*th trial signal and range of MUSIC orders *m* analysed in the iteration (see Fig. 1b), are obtained.

$$\overline{FI}_{m,R} = \frac{1}{N_t}\sum_{i=0}^{N_t} FI_{i,R} \text{ for } \mathrm{m} = 2, 3\ldots, 160 \tag{10}$$

where N_t is the number of trials for each rotor state. The minimum (m = 2) and the maximum value (m = 160) of *m* are consistent with Ref. [15].

2) Then, the difference between values computed as Eq. (10), for R1 and R2 rotor states, is calculated accordingly.

$$\Delta\overline{FI}_{m,incip} = \overline{FI}_{m,R1} - \overline{FI}_{m,R2} \text{ for } \mathrm{m} = 2, 3\ldots, 160 \tag{11}$$

3) Finally, these values are ordered following the univariate ordering of data

studied in Ref. [24]. Let the $\Delta\overline{FI}_{m,incip}$, be arranged in ascending order of magnitude as:

$$\Delta\overline{FI}_{incip(1)} \le \Delta\overline{FI}_{incip(2)} \le \ldots \le \Delta\overline{FI}_{incip(n-2)} \le \Delta\overline{FI}_{incip(n-1)} \le \Delta\overline{FI}_{incip(n)} \tag{12}$$

The *i*th $\Delta\overline{FI}_{incip(i)}$ is the so called *i*th order statistic, where the minimum is $\Delta\overline{FI}_{incip(1)}$, and the maximum is $\Delta\overline{FI}_{incip(n)}$. The MUSIC orders chosen are those which correspond to the following order statistics: $\Delta\overline{FI}_{incip(n)}$, $\Delta\overline{FI}_{incip(n-1)}$ and $\Delta\overline{FI}_{incip(n-2)}$.

4. Experimental setup

A squirrel cage IM by Siemens (model 1LA7083-4AA10), star connected and with two pole pairs, has been tested. The IM has the following plate characteristics: 0.75 kW, 400 V, 1.86 A, 50 Hz and 1395 rpm as full load speed. The squirrel cage rotor bars have a depth of 18 mm. A layout of the laboratory setup is shown in Fig. 4. A magnetic powder brake provides the mechanical load to the IM. The motor is tested under four different power supplies: direct on line and three inverters by ABB, WEG, and Telemecanique (TM), their models being ACS355, CFW-11 and Altivar 66, respectively. The three inverters are programmed with a scalar control, which is one of the most commonly used in industry [25]. The switching frequency is 4 kHz, except for the WEG inverter which is 5 kHz. Three rotor conditions are tested with each power supply: healthy (R1), partially BRB with a 9 mm depth drilled hole (R2) and a fully BRB (R3), as can be seen in Fig. 4. Two motor load levels are also established to determine their influence on the detection of the incipient rotor bar breakage. The resulting slip is 0.03 under a medium load and 0.05 at full load. The stator current is acquired by a LEM Hall-effect current transducer. Data are recorded by a National Instruments NI cDAQ-9174 base platform with an NI 9215 acquisition module. The sampling frequency is 50 kHz and the sampling time is 10 s.

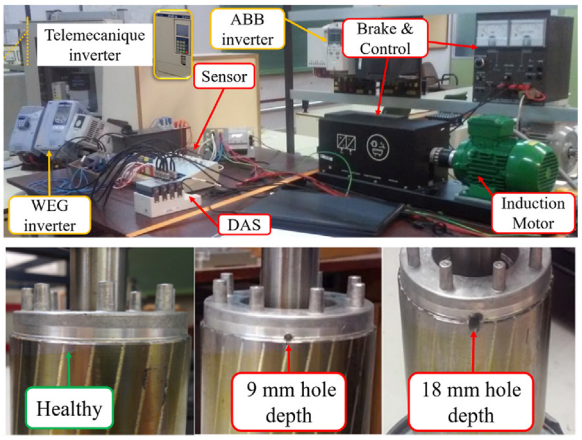

Fig. 4. General view of the laboratory set up with different rotor states shown in the lower part: from left to right: healthy (R1), partially BRB (R2), and fully BRB (R3), respectively.

5. Results

The first step of the proposed methodology includes the accurate location of BRB frequencies. Fig. 5 depicts the dispersion produced

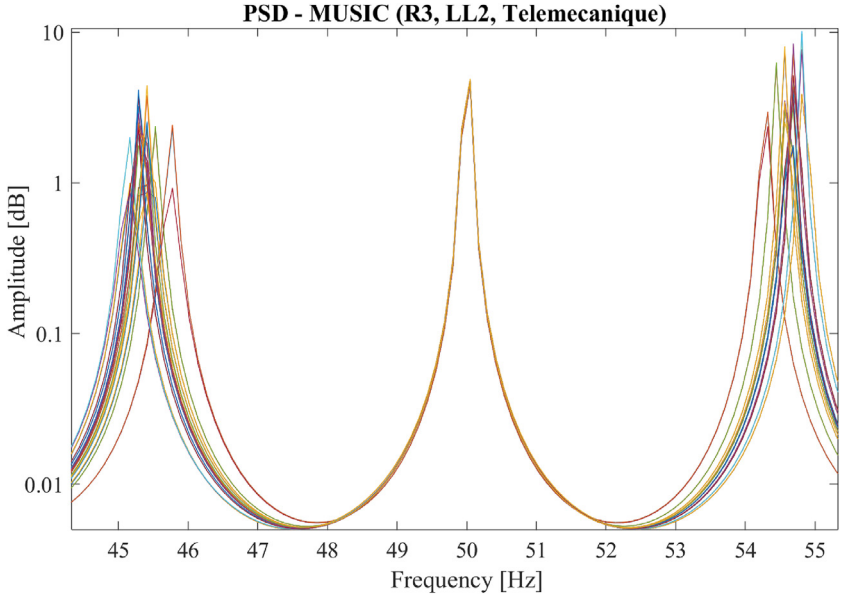

Fig. 5. Dispersion of the MUSIC spectra computed at different samples when the motor has a BRB, high load, and fed with a Telemecanique inverter.

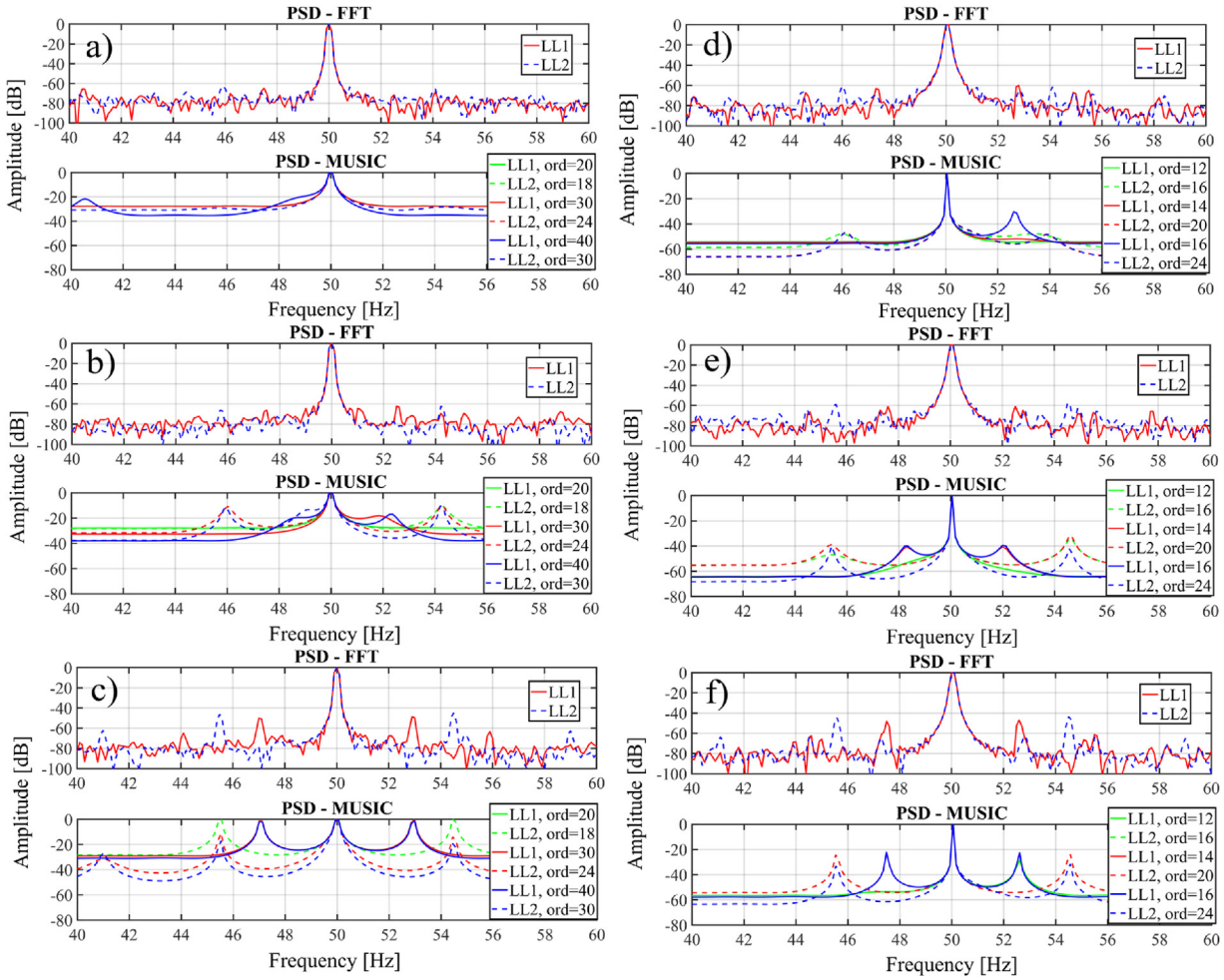

Fig. 6. FFT and MUSIC for the ABB and WEG supplies applied to the stator current of each motor state and load: (a) ABB, healthy, R1 (s1 = 0.03, s2 = 0.05); (b) ABB, partially broken bar, R2 (s1 = 0.0272, s2 = 0.047); (c) ABB, fully broken bar, R3 (s1 = 0.0299, s2 = 0.0556); (d) WEG, healthy, R1 (s1 = 0.035, s2 = 0.054); (e) WEG, partially broken bar, R2 (s1 = 0.0277, s2 = 0.0478) (f) WEG, fully broken bar, R3 (s1 = 0.0254, s2 = 0.0489).

for determining the BRB frequencies from different samples of the set of trials at one operating condition. In this case, signals belonging to a Telemecanique inverter-fed motor with one broken bar, under high load are shown. Once the BRB frequencies are located, in the second stage of the methodology, the fault severity can be estimated through FFT. These steps would apply for the remaining cases.

As an example, Figs. 6 and 7 show the PSD of some signals computed with MUSIC, for the BRB frequencies location, and with FFT for the severity estimation. These figures help to observe the discriminating capability with the methodology used. The FFT spectra show how the noise level complicates identification and extraction of fault signatures whereas the MUSIC algorithm improves the location of these components. Since MUSIC is sensitive to increments in fault severity, it provides a closer observation of the incipient BRB (R2) signatures. The above-mentioned dataset of stator current signals is analysed using the three chosen MUSIC orders, and is shown in Table 2. In this case, the fault signature considered is the sum of the LSH and RSH amplitudes [26,27].

Figs. 6a–c displays the PSD of some stator currents computed with FFT and MUSIC algorithms. Fig. 6a shows the PSD for the healthy case and Figs. 6b–c show the sideband frequencies for R2 and R3 fault severities for the ABB inverter-fed IM, respectively. In this particular case, the technique enables perfect discrimination between the different motor conditions and for both IM load levels. Following this procedure, results for the rest of the power supplies are obtained. Figs. 6d–f show the results for the WEG inverter case after applying the technique with the three parameters adopted. It can be seen that maintaining the same MUSIC orders produces differences in the detectability values for each fault severity. However, results summarized in Table 2 demonstrate that in the case of medium load levels (LL1), fault detectability values for the incipient BRB are not useful and significant. For the high load IM condition (LL2), they seem better for the R2 fault severity than those observed for the LL1.

Figs. 7a–c present the spectra of the stator current for the TM inverter case. It is interesting to point to the high noise level present in the FFT spectra, which hides the fault components in R2 severity. Even MUSIC is not able to display them. The presence of this high noise level makes this case the most difficult to analyse and only the full BRB case is detected.

The line-fed IM is the last case analysed. Figs. 7d–f undoubtedly show that the early BRB fault condition can be detected regardless of the IM loads considered. In this particular case, MUSIC manages to identify a partially broken bar with the three *m* orders considered.

Once the three MUSIC parameters are chosen from the iterative procedure, a final analysis is performed. The analysis results indicate that the most appropriate parameters are the following:

1) The order depends on the motor load level and the specific power supply used. The most discriminating orders for detect-

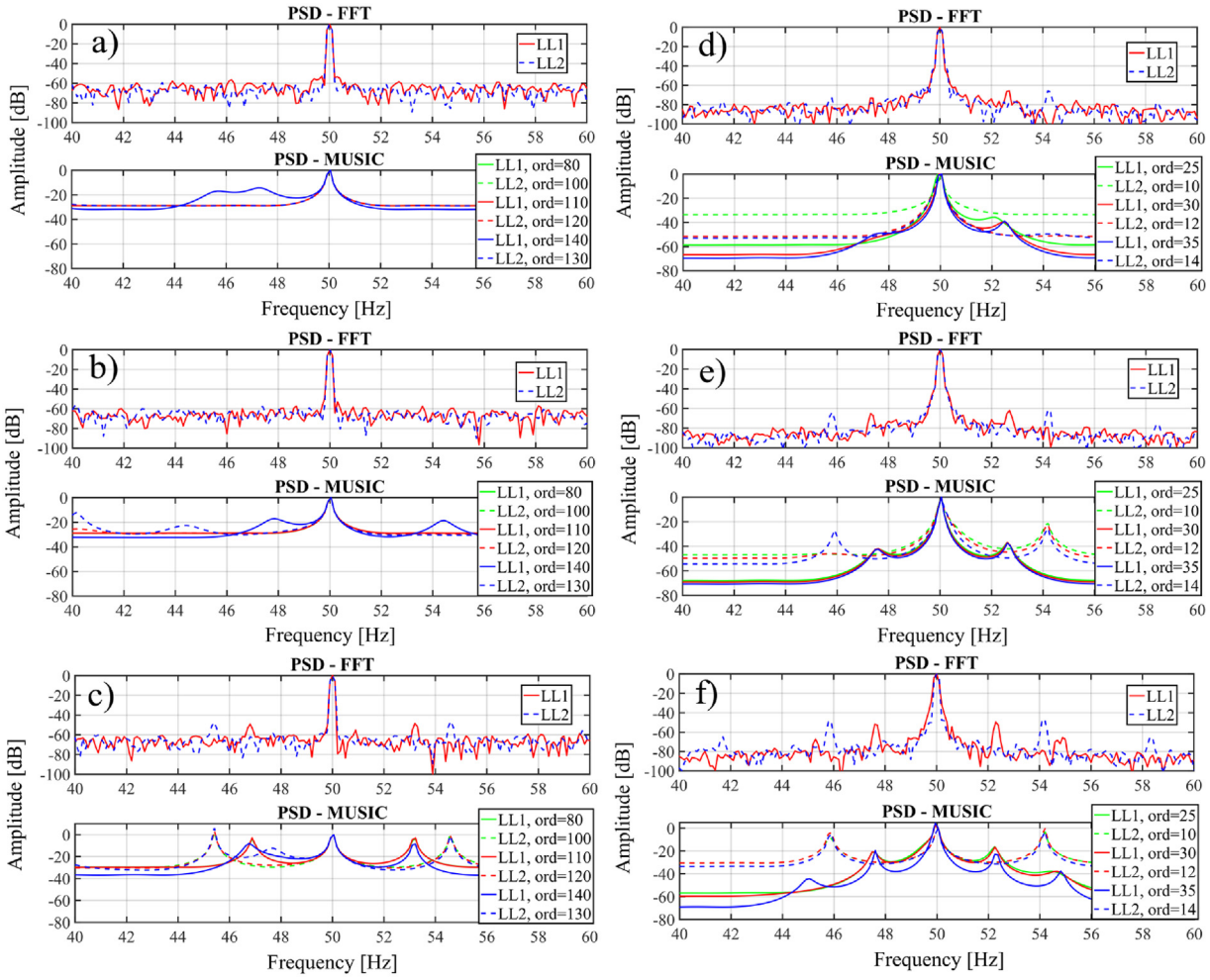

Fig. 7. FFT and MUSIC for the Telemecanique and line-fed supplies applied to the stator current of each motor state and load: (a) TM, healthy, R1 (s1 = 0.034, s2 = 0.047); (b) TM, partially broken bar, R2 (s1 = 0.0360, s2 = 0.043); (c) TM, fully broken bar, R3 (s1 = 0.0308, s2 = 0.0443); (d) Line, healthy, R1 (s1 = 0.0313, s2 = 0.0463); (e) Line, partially broken bar, R2 (s1 = 0.0281, s2 = 0.0445); (f) Line, fully broken bar, R3 (s1 = 0.023, s2 = 0.04).

ing BRB are those shown in Table 2. It has been experimentally observed that higher orders are better at discriminating between R1 and R2 fault conditions whereas this is not a favorable circumstance for the full BRB condition.

2) The window and overlapping lengths of samples 200 and 199 respectively, are sufficient for obtaining the spectra.

As can be deduced from Table 2, one of the weaknesses of the MUSIC pseudo-spectra is that the amplitudes obtained are a rough estimate of the real energy of the frequency components as stated in Ref. [12]. However, these peaks cannot be directly extracted from the PSD computed with FFT because it is necessary to know the rotor slip in advance and to acquire a large number of samples to obtain a good frequency resolution. Therefore, the required acquisition time is very long, and also these peaks can be hidden by high noise levels.

On the other hand, MUSIC offers the following advantages: (i) it requires a much smaller number of samples; (ii) it can provide a PSD free of noise, and (iii) this leads to better location of the fault related frequencies. There is a negative exception when the motor is supplied from a noisy inverter such as TM. Nevertheless, there are cases where the MUSIC pseudo-spectrum shows spurious frequencies, and identifying the fault harmonics is not straightforward. These are the discarded cases, whose fault frequencies do not appear in the MUSIC spectrum. Therefore, the results demonstrate that the type of power supply has a strong influence on the detectability of the incipient fault. The IM line-fed case is the easiest to detect. In addition, after examining all the tests with the proposed methodology, the three MUSIC orders chosen enable us to achieve a better study of each rotor condition separately, as they can be generalized for a wide set of signals. This experimental methodology shows that there is not a unique MUSIC order that enables us to obtain the proper information for all rotor conditions.

6. Conclusions

This paper presents an FD study based on the MUSIC algorithm, which provides results for noisy signals obtained from different power supplies. This analytical methodology comprises an iterative search of the algorithm parameters over an experimental set of trials. It has been observed that parameter choice depends on load level and the power supply considered. Furthermore, based on the laboratory analysis, a unique MUSIC order does not help us identify an incipient rotor fault. Thus, the three parameter selection enables us to identify (in some cases) intermediate severities between the healthy state and complete BRB when detecting rotor faults in squirrel-cage IM. The particularity of this study lies in the analysis of one-phase electric current stator signals with low SNR, coming from the inverter supply. This noise content, coming from different inverters, has been analysed in the context of its influence on FD. For steady-state approaches, it can be concluded that MUSIC provides better results than those obtained with FFT only

Table 2
Average detectability values for the full dataset after processing with FFT and MUSIC for the orders adopted under medium and high load conditions.

Power supply	Load level	MUSIC order	MUSIC $FI_{LSH} + FI_{RSH}$			FFT LSH + RSH		
			Rotor condition					
			R1	R2	R3	R1	R2	R3
ABB	LL1	20	0	1	59	−160	−129	−98
		30	0	4	59			
		40	1	7	58			
	LL2	18	1	19	71	−163	−127	−91
		24	10	30	70			
		30	15	41	69			
WEG	LL1	12	1	0	20	−152	−146	−95
		14	2	0	53			
		16	5	1	53			
	LL2	16	12	29	66	−153	−133	−89
		20	29	40	64			
		24	36	44	59			
TM	LL1	80	0	0	43	−128	−129	−100
		110	0	0	47			
		140	11	13	47			
	LL2	100	0	0	57	−129	−126	−95
		120	0	1	59			
		130	3	0	60			
Line-fed	LL1	25	3	9	18	−166	−143	−102
		30	4	13	27			
		35	5	13	30			
	LL2	10	0	1	46	−174	−131	−94
		12	0	4	52			
		14	10	11	59			

because the proposed method helps to locate the faulty frequency components with a smaller number of samples. However, the proposed method requires two steps and it could involve a limitation. Thus, for future research, it would be desirable to continue working to achieve a quantification of the incipient fault with MUSIC or another method in a single step.

Acknowledgments

This work was supported in part by the Mexican Council of Science and Technology (CONACyT), scholarship 598078; by a mobility grant from the Universidad de Valladolid, Spain; by the Spanish 'Ministerio de Economía y Competitividad' (MINECO) and FEDER program in the framework of the 'Proyectos I+D del Subprograma de Generación de Conocimiento, Programa Estatal de Fomento de la Investigación Científica y Técnica de Excelencia' (ref: DPI2014-52842-P); by the Universidad Autonoma de Queretaro Sabbatical Scholarship 2015-2016; by the Universidad de Guanajuato DAIP Grant 733/2016; and by the Universidad de Valladolid Grant for foreign professors in the doctoral program 2015–2016. WEG Iberia donated one of the inverters used in this work.

References

[1] R.H. Cunha-Palacios, I.N. Silva, A. Goedtel, W.F. Godoy, A comprehensive evaluation of intelligent classifiers for fault identification in three-phase induction motors, Electr. Power Syst. Res. 127 (2015) 249–258.
[2] R.Z. Haddad, E.G. Strangas, On the accuracy of fault detection and separation in permanent magnet synchronous machines using MCSA/MVSA and LDA, IEEE Trans. Energy Convers. 31 (2016) 924–934.
[3] O. Duque-Perez, L.A. Garcia-Escudero, D. Morinigo-Sotelo, P. Gardel, M. Perez-Alonso, Analysis of fault signatures for the diagnosis of induction motors fed by voltage source inverters using ANOVA and additive models, Electr. Power Syst. Res. 121 (2015) 1–13.
[4] J. Cusido, L. Romeral, J.A. Ortega, J.A. Rosero, A. Garcia-Espinosa, Fault detection in induction machines using power spectral density in wavelet decomposition, IEEE Trans. Ind. Electron. 55 (2008) 633–643.
[5] A. Naha, A.K. Samanta, A. Routray, A.K. Deb, A method for detecting half-broken rotor bar in lightly loaded induction motors using current, IEEE Trans. Instrum. Meas. 65 (2016) 1614–1625.
[6] M.E.H. Benbouzid, G.B. Kliman, What stator current processing-based technique to use for induction motor rotor faults diagnosis? IEEE Trans. Energy Convers. 18 (2003) 238–244.
[7] B. Ayhan, H.J. Trussell, On the use of a lower sampling rate for broken rotor bar detection with DTFT and AR-based spectrum methods, IEEE Trans. Ind. Electron. 55 (2008) 1421–1434.
[8] R.J. Romero-Troncoso, A. Garcia-Perez, D. Morinigo-Sotelo, O. Duque-Perez, R.A. Osornio-Rios, M.A. Ibarra-Manzano, Rotor unbalance and broken rotor bar detection in inverter-fed induction motors at start-up and steady-state regimes by high-resolution spectral analysis, Electr. Power Syst. Res. 133 (2016) 142–148.
[9] M.R. Mehrjou, N. Mariun, M.H. Marhaban, N. Misron, Rotor fault condition monitoring techniques for squirrel-cage induction machine—a review, Mech. Syst. Signal Process. 25 (2011) 2827–2848.
[10] B. Xu, L. Sun, L. Xu, G. Xu, Improvement of the Hilbert method via ESPRIT for detecting rotor fault in induction motors at low slip, IEEE Trans. Energy Convers. 28 (2013) 225–233.
[11] P. Stoica, R. Moses, Spectral Analysis of Signals, Pearson Prentice-Hall, 2005.
[12] Y.H. Kim, Y.W. Youn, D.H. Hwang, J.H. Sun, D.S. Kang, High-resolution parameter estimation method to identify broken rotor bar faults in induction motors, IEEE Trans. Ind. Electron. 60 (2013) 4103–4117.
[13] A. Garcia-Perez, R.J. Romero-Troncoso, E. Cabal-Yepez, R.A. Osornio-Rios, The application of high-resolution spectral analysis for identifying multiple combined faults in induction motors, IEEE Trans. Ind. Electron. 58 (2011) 2002–2010.
[14] L.A. Pereira, D. Fernandes, D.S. Gazzana, F.B. Libano, S. Haffner, Performance evaluation of nonparametric, parametric, and the MUSIC methods to detection of rotor cage faults of induction motors, Proc. 2006 IEEE 32nd Annual Conference on Industrial Electronics, IECON (2006) 5005–5010.
[15] G. Trejo-Caballero, H. Rostro-Gonzalez, R.J. Romero-Troncoso, C.H. Garcia-Capulin, O.G. Ibarra-Manzano, J.G. Avina-Cervantes, A. Garcia-Perez, Multiple signal classification based on automatic order selection method for broken rotor bar detection in induction motors, Electr. Eng. (2016) 1–10.
[16] I.P. Georgakopoulos, E.D. Mitronikas, A.N. Safacas, Detection of induction motor faults in inverter drives using inverter input current analysis, IEEE Trans. Ind. Electron. 58 (2011) 4365–4373.
[17] K. Yahia, A.J.M. Cardoso, S.E. Zouzou, S. Gueddidi, Broken rotor bars diagnosis in an induction motor fed from a frequency converter: experimental research, Int. J. Syst. Assur. Eng. Manag. 3 (2012) 40–46.
[18] N.H. Kim, W.S. Baik, M.H. Kim, C.H. Choi, Rotor fault detection system for the inverter driven induction motor using current signals, J. Power Electron. 9 (2009) 224–231.
[19] B. Kim, K. Lee, J. Yang, S.B. Lee, E.J. Wiedenbrug, M.R. Shah, Automated detection of rotor faults for inverter-fed induction machines under standstill conditions, IEEE Trans. Ind. Appl. 47 (2011) 55–64.

[20] V. Ghorbanian, J. Faiz, A survey on time and frequency characteristics of induction motors with broken rotor bars in line-start and inverter-fed modes, Mech. Syst. Signal Process. 54–55 (2015) 427–456.
[21] J. Faiz, V. Ghorbanian, B.M. Ebrahimi, EMD-based analysis of industrial induction motors with broken rotor bars for identification of operating point at different supply modes, IEEE Trans. Ind. Inf. 10 (2014) 957–966.
[22] M.C. Piazza, M. Pucci, Techniques for efficiency improvement in PWM motor drives, Electr. Power Syst. Res. 136 (2016) 270–280.
[23] C. Hargis, B.G. Gaydon, K. Kamash, The detection of rotor defects in induction motors, Proc. IEEE International Conference on Electrical Machines, Design and Application (1982) 216–220.
[24] D.C. Montgomery, Design and Analysis of Experiments, John Wiley & Sons, 2006.
[25] T.H. dos Santos, A. Goedtel, S.A.O. da Silva, M. Suetake, Scalar control of an induction motor using a neural sensorless technique, Electr. Power Syst. Res. 108 (2014) 322–330.
[26] A. Bellini, F. Filippetti, G. Franceschini, C. Tassoni, G.B. Kliman, Quantitative evaluation of induction motor broken bars by means of electrical signature analysis, IEEE Trans. Ind. Appl. 37 (2001) 1248–1255.
[27] G.B. Kliman, R.A. Koegl, J. Stein, R.D. Endicott, M.W. Madden, Noninvasive detection of broken bars in operating induction motors, IEEE Trans. Energy Convers. 3 (1988) 873–879.